Weakly Nonlinear Theory

Chrysovalantis Thomopoulos

Supervised by Philip Hall
School of Mathematical Sciences, Monash University

21 October, 2022

Abstract

A weakly nonlinear theory describing the effect of boundary forcing and transpiration on flow is examined. Vortex wave interactions are explained as well as the linear stability theory in order for the nonlinear stability theory to be understood and used to our advantage. The derivation of the vortex wave interaction equations takes place for both plane and pipe. Solutions that arise characterise the possible bifurcations that our system undergoes because of the amplitude of the introduced perturbations. Finally, results are analyzed and discussed.

Contents

Chapter 1

Introduction and Background

The motivation behind this piece of work is to further amalgamate boundary forcing and transpiration with the vortex-wave interaction theory in shear flows. We focus on the uniform shear flow in both an unbounded plane and a pipe under the influence of boundary forcing or transpiration. When considering the boundary forcing case a small amplitude, stationary, aligned wavy wall is set as y or r respectively and for the transpiration case fluid is injected into our flow in a flat plane. For the plane case, the wall wavelength is set to be our lengthscale and when compared to the wall normal lengthscale it is considered to be small. Additionally, the high Reynolds number is based on the forcing wavelength and the friction velocity $u_s = \sqrt{\nu u'(0)}$ with ν being the kinematic viscosity. As for the pipe case, the specified wall undulation amplitude is small compared to the boundary layer thickness at the wall and the Reynolds number is dependent on the mean pipe radius and the maximum unperturbed velocity.

Work conducted in Ruban, 1985 and Raposo et al., 2019 for which boundary forcing and more specifically wavy walls were used as a receptivity mechanism for unstable flows does not correlate with what we are doing. Additionally, the same can be said about Ni, 2019 in which sensitivity analysis is conducted. Alternatively, we utilize boundary forcing for the generation of the instability itself in order to control the transition.

Wavy walls as we will refer to them have been used extensively for mixing by heat transfer specialists. Extensive research has been conducted by Kandlikar, 2008, Comini et al., 2003 and Guzmán et al., 2009, both analytically and computationally. Further, wavy walls can play an integral part in reducing drag for airfoils as seen in Gad-el-Hak, 1990 where the speed is considered to be low. Wavy walls can also affect the transition to turbulence as seen in Ozcakir et al., 2022, which we will utilize. Unfortunately, some of these discoveries can not be used yet in a real life setting apart from a small aerodynamic and heat optimizing turbine. Implementation in civilian aircrafts for example would be a hard feat because of the excessive weight needed to create the turbines or wings.

Transpiration has also been widely used to control the transition in laminar boundary layers Balakumar and Hall, 1999 where it takes the form of uniform suction. Prevention of the transition is entirely possible but the power for an enormous pump would be cost deficient. Another setting in which transpiration is also used are hypersonic flows like in Gülhan and Braun, 2010 where transpiration is utilized for cooling, another common use.

Multiple mechanisms have been discussed and theorised in the past in regards to nonlinear interactions at a high Reynolds number. The basis for the vortex wave interactions (VWI) that we will be focusing on emerge from Hall and Smith, 1991 which explain a plethora of Tollmien-Schlichting and Rayleigh-wave boundary layer nonlinear interactions. We will plunge into one of the simpler shear flow cases for which theory has been established from Hall, 2020 and Hall and Ozcakir, 2021. Dr. Hall and Ozcakir came up with the idea that a small self interacting wave in the viscous boundary layer gives rise to a roll flow. The rolls keep growing in amplitude but can only be sustained in the boundary layer because of the Reynolds stress terms. In response the roll flow initiates a streak which is neutrally unstable to the wave. Thus, an endless cycle is created as can be seen in figure 1.1. It is also important to point out that the streak flow is bigger by a factor of the Reynolds number compared to the roll flow in the critical layer. This proves crucial in understanding.

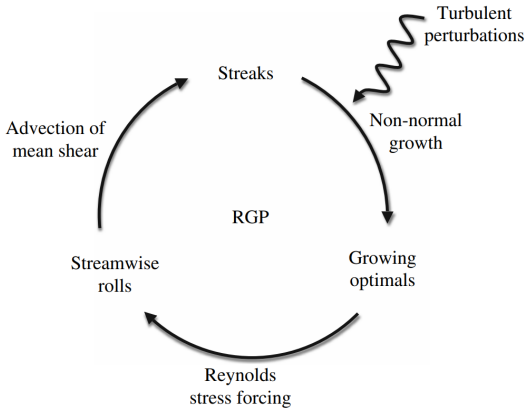

Figure 1.1: Roll-Streak Flow

The main paper that we will base our own work and take inspiration from for the plane case is Hall, 2022. Hall described multiple cases that we do not look into such as the linear stability theory for the bounded channel, the propagating wave and oblique wavy wall configurations. This paper focuses on the nonlinear stability theory of the unbounded channel, thus a plane in the presence of the stationary aligned wavy wall. In the same spirit Hall and Ozcakir, 2021 conducted the linear stability theory for the briefly aforementioned pipe setup for which they considered different types of roughness, $3D$ as well as limits of small and wave roughness which we do not focus on.

The nonlinear stability method that is used originates from Taylor, 1923 and was further analyzed by Stuart, 1971.It will be discussed prior to the presentation of our work and findings in the remaining of Chapter 1. The topic of discussion in § 2 is the cartesian VWI system from Hall, 2022 for the plane alongside the results for the aligned stationary wavy wall and transpiration cases. In §3 we proceed to explain the cylindrical VWI system but this time for the equivalent pipe case from Hall and Ozcakir, 2021 and display our results for the aligned stationary wavy wall. Finally, in Chapter 4 we discuss further and draw some conclusions.

1.1 Linear Stability Theory

Linear stability theory revolves around the introduction of perturbations to a stable system with the intention of understanding if the flow in question remains laminar or transitions to turbulence. We start off with the incompressible *Navier-Stokes* equations

$$\begin{aligned} \nabla \cdot \mathbf{u} &= 0, \\ \frac{\partial \mathbf{u}}{\partial t} + \mathbf{u} \cdot \nabla \mathbf{u} &= -\frac{1}{\rho}\nabla p + \nu \nabla^2 \mathbf{u}, \end{aligned} \tag{1.1.1}$$

and continue by nondimensionalizing them. We set $\hat{x} = Lx, \hat{y} = Ly, \hat{z} = Lz$ and $\hat{t} = \frac{L}{V}t$ with L being the characteristic scale of the body and V the modulus of the free-stream velocity vector. Furthermore, we set the Reynolds number to be $Re = \frac{VL}{\nu}$ and drop the hat notation resulting into

$$\begin{aligned} \nabla \cdot \mathbf{u} &= 0, \\ \frac{\partial \mathbf{u}}{\partial t} + \mathbf{u} \cdot \nabla \mathbf{u} &= -\nabla p + \frac{1}{Re}\nabla^2 \mathbf{u}. \end{aligned} \tag{1.1.2}$$

Now based on Stuart, 1971 and Drazin, 2002 we assume that a steady flow takes place with the time independent solutions being $\bar{u}(x, y, z)$; $\bar{v}(x, y, z)$; $\bar{w}(x, y, z)$ and $\bar{p}(x, y, z)$. The perturbations then take the form of

$$\begin{aligned} u &= \bar{u} + \delta * u'(x, y, z, t), \\ v &= \bar{v} + \delta * v'(t, x, y, z), \\ w &= \bar{w} + \delta * w'(t, x, y, z), \\ p &= \bar{p} + \delta * p'(t, x, y, z), \end{aligned} \tag{1.1.3}$$

with a small amplitude δ. The boundary value problem admits a trivial solution indicating the need of a different approach. We transform our problem into an eigenvalue one by separating our variables with the assistance of Laplace Transforms resulting into the so called normal modes

$$\begin{aligned} \mathbf{u}'(x, y, z, t) &= e^{\sigma t}\tilde{\mathbf{u}}(x, y, z), \\ p'(x, y, z, t) &= e^{\sigma t}\tilde{p}(x, y, z). \end{aligned} \tag{1.1.4}$$

The eigenvalues σ take a complex form and constitute a spectrum which will allow us to understand the nature of the flow which depends solely on the sign of the eigenvalues in the complex plane. The time dependent terms are then collected and expanded

$$e^{\sigma t} = e^{(\sigma_r + i\sigma_i)t} = e^{\sigma_r t}[\cos(\sigma_i t) + isin(\sigma_i t)], \tag{1.1.5}$$

so the perturbations consist of an amplitude $e^{\sigma_r t}$ and frequency σ_i. It is important to point out that when all $\sigma_r < 0$ our flow returns to its steady state despite the introduction of perturbations. On the other hand if a single σ_r is positive then our flow is deemed unstable and the perturbations will grow over time allowing another possibly turbulent state to establish itself.

1.2 Taylor Vortices and Nonlinear Stability Theory

The experiments and analysis that were conducted by Stuart, 1971; Kogelman and DiPrima, 1970 and Eckhaus, 1965 proved that improvements to the linear stability theory were possible for refined results. Taylor's experiment involves the flow between concentric rotating circular cylinders with the inner one in rotation whilst the outer is in rest. When the angular speed of the inner rotating cylinder exceeds a critical value periodic toroidal vortices known as Taylor vortices appear instead of turbulent structures based on figure 1.2

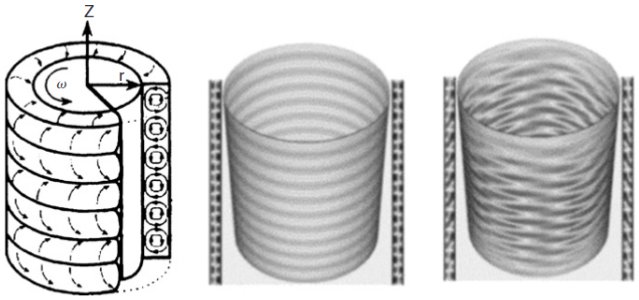

Figure 1.2: Taylor Vortices

The measure that is used is the Taylor number $T = \frac{\Omega_1 R_1 d^3}{\nu^2}$ with R_1 being the radius, Ω_1 the angular speed of the inner cylinder, ν the kinematic viscosity and d the distance between the two cylinders. It represents the ratio of the centrifugal forces compared to the viscous forces with T_c the critical point at which this bifurcation takes place ignoring the second bifurcation point where the Taylor vortices become wavy and thus turbulent.

Figure 1.3 from Stuart, 1971 depicts the neutral curve of the linear stability theory alongside its azimuthal expansion with the small amplitude ϵ. The area under the curve

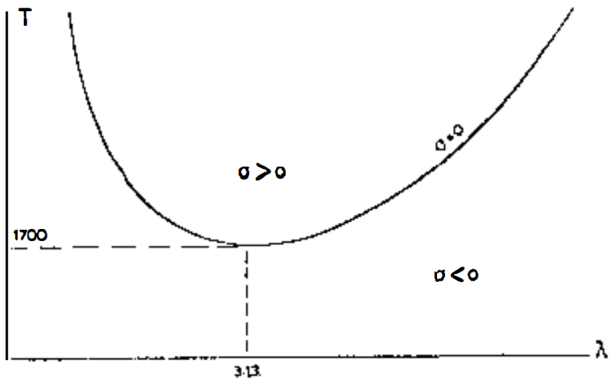

Figure 1.3: Neutral Curve of LST.

represents the aforementioned stable area where all $\sigma < 0$ and above it is the unstable area where one or more σ eigenvalues are positive. When using a nonlinear azimuthal

expansion, with $v_{20}(r)$ being the the mean-flow correction,

$$\begin{aligned} v_\theta =& v_0(r) + \epsilon v_1(r)\cos(\lambda z) + \epsilon^2[v_{21}(r) + v_{22}(r)\cos(2\lambda z)] \\ &+ \epsilon^3[v_{31}(r)\cos(\lambda z) + v_{33}(r)\cos(3\lambda z)] + \dots, \end{aligned} \tag{1.2.1}$$

based on the work from Eckhaus, 1965 two other mathematicians Kogelman and DiPrima, 1970 exhibited their newly found neutral curve. In Figure 1.4 the linear stability theory curve denoted as I and the nonlinear stability theory curve denoted as II overlay. The

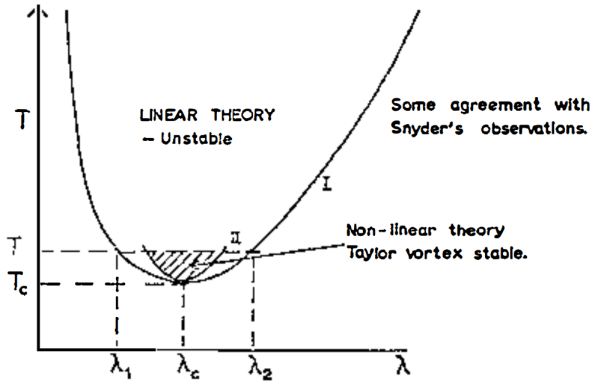

Figure 1.4: Neutral Curve of NLST/LST.

shaded section in the $\sigma > 0$ area portrays the Taylor vortices. Despite the fact that some of our eigenvalues are positive, the flow does not transition to turbulence aligning with the findings of Taylor's experiments and contradicting the linear stability theory. The use of the nonlinear stability theory is therefore preferred because of its accuracy.

1.3 Stuart-Landau Equation

With the use of the nonlinear stability theory an amplitude equation arises according to Stuart, 1971 and Drazin, 2002. The Stuart-Landau equation distinguishes our dynamics around the bifurcation point and tends to frequently appear with weakly nonlinear problems.

$$\frac{dA}{dt} = \sigma_c A - \beta A|A|^2. \tag{1.3.1}$$

The constants σ_c and β can be complex. We continue by setting $A(t) = r(t)e^{i\theta(t)}$ following a popular method from Eckhaus, 1965 and solve the equation.

Real Constants

When $\sigma_c, \theta \in \mathbb{R}$ then the system is

$$r' = \sigma_c r - \beta r^3 \quad and \quad \theta' = 0. \tag{1.3.2}$$

Since $\theta' = 0$ that indicates that we have a pitchfork bifurcation. A supercritical pitchfork bifurcation appears when $\beta > 0$ and a subcritical pitchfork bifurcation when $\beta < 0$.

Imaginary Constants

When $\sigma_c, \theta \in \mathbb{C}$ then the system is

$$\begin{aligned} r' &= \sigma_{cr} r - \beta_r r^3, \\ \theta' &= \sigma ci + -\beta_i r^2. \end{aligned} \tag{1.3.3}$$

Like in the real case above when $\beta_r > 0$ a supercritical Hopf bifurcation takes place and when $\beta_r < 0$ we have a subcritical Hopf bifurcation regardless of the sign of σ_{cr}. Further, σ_{cr} determines the direction of our spiral while the σ_{ci} determines its direction. We will not be going into more detail but additional information can be found in Glendinning, 1994.

Chapter 2

Plane Cases

The first case that we will be tackling is the unbounded plane and we therefore have to focus on the continuity equation

$$\nabla \cdot \hat{\mathbf{u}} = \frac{\partial \hat{u}}{\partial x} + \frac{\partial \hat{v}}{\partial y} + \frac{\partial \hat{w}}{\partial z}, \tag{2.0.1}$$

alongside the *Cartesian Navier-Stokes*

$$\frac{D\hat{\mathbf{u}}}{Dt} = -\nabla p + \frac{1}{Re}\nabla^2 \hat{\mathbf{u}}. \tag{2.0.2}$$

Here $\hat{u}$, $\hat{v}$ and $\hat{w}$ are the x, y and z velocity field components respectively whilst $\hat{p}$ is the pressure and Re is the Reynolds number which as mentioned in Chapter 1 is dependent on the friction velocity like so

$$Re = \frac{R_f^2}{4\pi^2}, \tag{2.0.3}$$

$$Re_f = \frac{u_s b}{nu}. \tag{2.0.4}$$

As for the material derivative, it is set to be

$$\frac{D}{Dt} = \frac{\partial}{\partial t} + \hat{\mathbf{u}} \cdot \nabla, \tag{2.0.5}$$

and b is our forcing wavelength.

2.1 VWI Equations

For the boundary forcing case we set the wavy wall according to Hall, 2022 to be

$$y = 2\epsilon \cos\big(\alpha x + \beta z - \frac{\omega t}{Re^{1/3}}\big), \tag{2.1.1}$$

with the wave propagation angle being

$$\Theta = \tan^{-1}(\frac{\alpha}{\beta}). \tag{2.1.2}$$

As for the transpiration case, we assume that the wall is flat and fluid is injected at $y = 0$ like so

$$\hat{v} = 2\delta \cos\big(ax + \beta z - \frac{\omega t}{R^{1/3}}\big). \tag{2.1.3}$$

Both δ and ϵ are considered small compared to the boundary layer thickness $R^{-1/3}$ as well as our wavelengths, a usual assumption based on Smith, 1982. In this paper we will take the simpler case known as the aligned stationary wave case for which $\beta = \omega = 0$ with the streamwise wavelength α the only one remaining. We can now advance to the equations of motion for the plane and subsequently its correction at the wall layer, a theme which is prominent in our work.

The nonlinear system that we will be focusing on can be found in Hall, 2022. We will derive the system ourselves for the understanding of the reader and then proceed to apply the method of nonlinear stability theory. Lets suppose we have a unidirectional shear flow $(y, 0, 0)$ with $y = O(1)$ and introduce perturbations in the form of

$$\hat{\mathbf{u}} = (y, 0, 0) + \Big(u(y, z), \frac{v(y, z)}{Re}, \frac{w(y, z)}{Re}\Big), \quad p = \frac{p(y, z)}{Re^2}. \tag{2.1.4}$$

The system that follows if we insert our expansions in (2.0.2) is the following

$$\frac{\partial v}{\partial y} + \frac{\partial w}{\partial z} = 0, \tag{2.1.5}$$

$$\frac{\partial^2 u}{\partial y^2} + \frac{\partial^2 u}{\partial z^2} = v + v\frac{\partial u}{\partial y} + w\frac{\partial u}{\partial z}, \tag{2.1.6}$$

$$\frac{\partial^2 v}{\partial y^2} + \frac{\partial^2 v}{\partial z^2} = \frac{\partial p}{\partial y} + v\frac{\partial v}{\partial y} + w\frac{\partial v}{\partial z}, \tag{2.1.7}$$

$$\frac{\partial^2 w}{\partial y^2} + \frac{\partial^2 w}{\partial z^2} = \frac{\partial p}{\partial z} + v\frac{\partial w}{\partial y} + w\frac{\partial w}{\partial z}, \tag{2.1.8}$$

with the condition $u \to (0, 0, 0)$ at $y \to \infty$. Next,we focus on the wall layer for which we set a new scaled wall layer variable $\zeta = Re^{1/3}y$ for simplicity. Our new velocity field expansion based on Hall, 2022, takes the form of

$$\hat{u} = \frac{\zeta\lambda}{R^{1/3}} + \cdots + \Delta\big(U(\zeta, z)E + c.c\big) + \cdots \tag{2.1.9}$$

$$\hat{v} = \frac{v_m(\zeta, z)}{R^{4/3}} + \cdots + \frac{\Delta}{R^{1/3}}\big(V(\zeta, z)E + c.c\big) + \cdots \tag{2.1.10}$$

$$\hat{w} = \frac{w_m(\zeta, z)}{R} + \cdots + \big(\Delta(\zeta, z)E + c.c\big) + \cdots \tag{2.1.11}$$

$$\hat{p} = \frac{p_m(\zeta, z)}{R^2} + \cdots + \frac{\Delta}{R^{1/3}}\big(P(z)E + c.c\big) + \cdots \tag{2.1.12}$$

$$\tag{2.1.13}$$

with $\mathbf{u}_m$ being the mean flow corrections, $c.c$ represent the complex conjugates, $E = exp\big(i(\alpha x - \frac{\omega t}{R^{1/3}})\big)$, $\lambda(z) = \hat{u}_y(0, z)$ is our wall shear and the wave pressure is

dependent solely on z. Inserting them into (2.0.2) we acquire the wall layer system

$$i\alpha U+V_\zeta + W_z = 0, \tag{2.1.14}$$
$$-i\omega U + i\alpha\lambda\zeta U + \lambda V + \zeta W\lambda' = -i\alpha P + U_{\zeta\zeta}, \tag{2.1.15}$$
$$-i\omega W + i\alpha\lambda\zeta W = -P + z + W_{\zeta\zeta}, \tag{2.1.16}$$

with the inhomogeneous conditions for the boundary forcing case at the wall being $U_0 = -\lambda\Gamma e^{i\beta z}$, $V_0 = -i\omega\Gamma e^{i\beta z}$, $W_0 = 0$ and the transpiration case $U_0 = 0$, $V_0 = \Lambda e^{i\beta z}$, $W_0 = 0$. We will not delve into the working by Hall, 2022 because the primary focus of this paper revolves around the nonlinear stability theory. Instead we will mention that Hall discovered the wave pressure equation and the wall conditions to be

$$\frac{d^2P}{dz^2} - F\frac{\lambda'}{\lambda}\frac{dP}{dz} - \alpha^2 P = -\alpha\omega U_0 - \frac{i\alpha\sigma^{2/3}Ai'(\xi_0)}{\kappa}U_0 - \sigma V_0, \tag{2.1.17}$$
$$y = (0,0,w(0)) =(0,0,-\frac{1}{3}(\frac{1}{\lambda^2}\frac{\partial}{\partial z}[|P|^2 + \alpha^{-2}|P_z|^2])), \tag{2.1.18}$$

with

$$\sigma = -i\alpha\lambda, \qquad \xi_0 = -\frac{i^{1/3}\omega}{[\alpha\lambda]^{3/2}}, \qquad \kappa = \int_{\xi_0}^{\infty} Ai(\eta)\,d\eta, \tag{2.1.19}$$

$$F = \frac{1}{2}\Big(3 + \frac{\xi_0 Ai'(\xi_0)}{Ai(\xi_0)}\big[1 + \frac{\kappa\xi_0}{Ai'(\xi_0)}\big]\Big). \tag{2.1.20}$$

Therefore, for our case where $\beta = \omega = 0$ the respective wavy wall and transpiration wave pressure equations are

$$\frac{d^2P}{dz^2} - \frac{3}{2}\frac{\lambda'}{\lambda}\frac{dP}{dz} - a^2 P = 3\Gamma\sigma^{5/3}Ai'(0), \tag{2.1.21}$$
$$\frac{d^2P}{dz^2} - \frac{3}{2}\frac{\lambda'}{\lambda}\frac{dP}{dz} - a^2 P = -\sigma\Lambda. \tag{2.1.22}$$

2.2 Expansions and Final System

Having summarised the nonlinear system of equations that we will be workings on we can proceed to the nonlinear expansions that arise from Eckhaus, 1965 and Hall, 2022.

$$\begin{aligned}\mathbf{u} = {}& \delta A(\tau)\Big(u_1(y)\cos(kz), v_1(y)\cos(kz), w_1(y)\sin(kz)\Big)\\ &+ \delta^2 A(\tau)^2\Big(u_2(y)\cos(2kz) + u_M(y), v_2(y)\cos(2kz), w_2(y)\sin(2kz)\Big)\\ &+ \delta^3 A(\tau)^3\Big(u_{31}(y)\cos(kz), v_{31}(y)\cos(kz), w_{31}(y)\sin(kz)\Big)\\ &+ \delta^3 A(\tau)^3\Big(u_{32}(y)\cos(3kz), v_{32}(y)\cos(3kz), w_{32}(y)\sin(3kz)\Big)\\ &+ \delta^3 A'(\tau)\Big(u_{33}(y)\cos(kz), v_{33}(y)\cos(kz), w_{33}(y)\sin(kz)\Big).\end{aligned} \tag{2.2.1}$$

It is important to note that u_M is the mean-flow correction that emerges from the Reynolds stresses and k is the spanwise wavenumber. We assume the u and v periodic components to be odd in terms of z whilst w is even. Also, we set

$$\tau = \delta^2 t, \qquad \frac{d}{dt} = \delta^2 \frac{d}{d\tau}, \tag{2.2.2}$$

which will allow us to isolate the $A'(\tau)$ terms in the third order. We also know that on our linear neutral curve our amplitude is a constant and thus we can manipulate that fact and reintroduce a time variable into our equations, more specifically the slow time variable τ. We further simplify our system of equations by firstly differentiating (2.1.7) by $-\partial_z$ and (2.1.8) by ∂_y. We add the altered (2.1.7) and (2.1.8) in order to cancel the pressure out and differentiate the newly acquired equation by ∂_z whilst taking advantage of the continuity equation (2.1.5). Finally, we add the slow time component to the linear part of our $v(y,z)$ and $u(y,z)$ equations resulting into a new system.

$$(\nabla^2 - \frac{\partial}{\partial \tau})\nabla^2 v = \frac{\partial^2 J_2}{\partial z^2} - \frac{\partial}{\partial y}\big(\frac{\partial J_3}{\partial z}\big), \tag{2.2.3}$$

$$(\nabla^2 - \frac{\partial}{\partial \tau})u = v + J_1, \tag{2.2.4}$$

$$\frac{\partial v}{\partial y} + \frac{\partial w}{\partial z} = 0, \tag{2.2.5}$$

with boundary conditions

$$\mathbf{u} = (0,0,0) \quad \text{at} \quad y \to \infty, \tag{2.2.6}$$

$$\mathbf{u} = (0,0,-\frac{1}{3}(\frac{1}{\lambda^2}\frac{\partial}{\partial z}[|P|^2 + \alpha^{-2}|P_z|^2])) \quad \text{at} \quad y = 0. \tag{2.2.7}$$

Notice that the linear part of (2.2.3) is solely in terms of $v(y,z)$, a fact which will allow us to solve the system. Also, the J terms are the nonlinear parts that contribute to the RHS of our equations with

$$J_1 = v\frac{\partial u}{\partial y} + w\frac{\partial u}{\partial z}, \tag{2.2.8}$$

$$J_2 = v\frac{\partial v}{\partial y} + w\frac{\partial v}{\partial z}, \tag{2.2.9}$$

$$J_3 = v\frac{\partial w}{\partial y} + w\frac{\partial w}{\partial z}. \tag{2.2.10}$$

2.3 Velocity Field Terms

The velocity field for both the wavy wall and transpiration cases is the same. We will insert our expansions and gather orders of δ, δ^2 and δ^3 while ignoring $\cos(3kz)$ and higher order wavelength terms. We will obtain the v terms first

$$v_i = v_h + v_p = c_1 e^{-\bar{k}y} + c_2 y e^{-\bar{k}y} + c_3 e^{\bar{k}y} + c_4 y e^{\bar{k}y} + v_p, \tag{2.3.1}$$

with $i = 1,\ 2,\ M\ ,\ 31,\ 33$, the c's being constants and $\bar{k} = k,\ 2k\ ,\ 3k$. The particular solutions will always have a negative exponential for which we do not have to worry

about as $y \to \infty$. We apply the boundary condition at $y \to \infty$ ridding ourselves of the positive exponentials from v_h and consecutively apply no slip in order for one constant F_i to remain. From there we can uncover w_i from the continuity equation and then u_i which takes the form of

$$u_i = u_h + u_p = c_1 e^{-ky} + c_2 e^{ky} + l(k,y)e^{-2ky} + u_p, \tag{2.3.2}$$

where $l(k,y)$ is a polynomial in terms of k and the particular solution u_p contains negative exponentials. The condition at infinity and no slip are once again applied to give u_i. Having explained our general methodology we can now go ahead with our plan. The $O(\delta)$ system is as follows but can also be seen in Hall, 2022 for further reference

$$\begin{aligned} &(\frac{d^2}{dy^2} - k^2)u_1 = v_1, \\ &(\frac{d^2}{dy^2} - k^2)^2 v_1 = 0, \\ &w_1 = -\frac{1}{k}v_1'. \end{aligned} \tag{2.3.3}$$

Solving the ODE system alongside the boundary conditions $u_1, v_1, w_1 = 0$ at $y \to \infty$ and$u_1 = v_1 = 0$ at $y = 0$ we obtain the functions

$$v_1 = ye^{-ky}4k^2, \qquad u_1 = -(y + ky^2)e^{-ky}, \qquad w_1 = -4ke^{-ky}(1 - ky), \tag{2.3.4}$$

alongside $F_1 = k$ from the normalization $w'(0) = 1$ which further simplifies our work. We plot the velocity field functions against y at this order in figure 2.1 to check their validity. We repeat the same process and collect the $O(\delta^2)$ and $O(\delta^2 \cos(2kz))$ terms resulting into

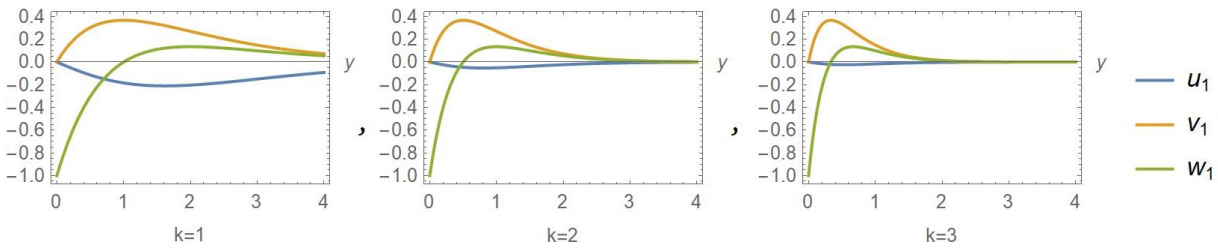

Figure 2.1: Linear velocity functions for varying k.

$$\frac{d^2(u_M)}{dy^2} = \frac{1}{2}(u_1 v_1)', \qquad (\frac{d^2}{dy^2} - 4k^2)u_2 = v_2 + \frac{1}{2}(v_1 u_1' - u_1 v_1'), \tag{2.3.5}$$

$$(\frac{d^2}{dy^2} - 4k^2)^2 v_2 = -((v_1')^2 - v_1 v_1'')', \qquad w_2 = -\frac{1}{2k}v_2'. \tag{2.3.6}$$

It is not surprising that a sole ODE arises for the mean flow correction of the x coordinate at $O(\delta^2)$ because of its lack of presence in (2.2.3) and (2.2.5). Solving the system once more with the aforementioned boundary conditions we attain the wanted functions which

can be seen below

$$u_M = \frac{-5 + e^{-2ky}\big(5 + 2ky(5 + ky(5 + 2ky))\big)}{64k^3}, \tag{2.3.7}$$

$$v_2 = -\frac{1}{16}e^{-2ky}y(1 + 16F_2 + ky), \tag{2.3.8}$$

$$w_2 = -\frac{e^{-2ky}\big(-1 + 2k^2y^2 + 16F_2(-1 + 2ky)\big)}{32k}, \tag{2.3.9}$$

$$u_2 = \frac{1}{1526k^2}e^{-2ky}\big(-3 - 96F_2(1 + 2ky) + 2ky(-3 + 4ky)\big), \tag{2.3.10}$$

with F_2 being the constant of this order. F_2 is dependent on α as well as k and is found from the inhomogeneous wall condition. Therefore, there are two different F_2 polynomials for each case. We now plot the velocity field at this order for the undulation constant with varying α and k in figure 2.2.

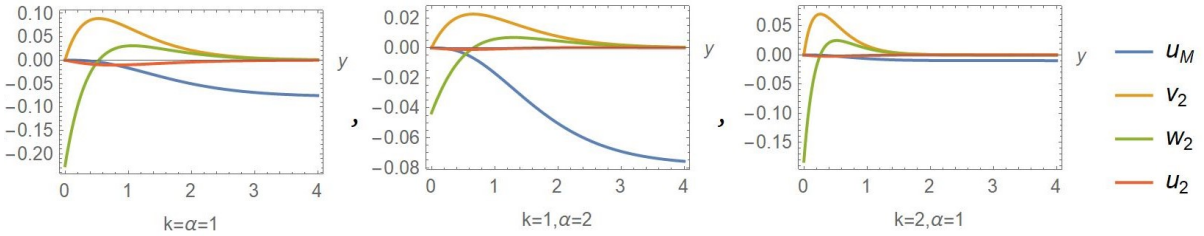

Figure 2.2: Second order wavy wall velocity functions for varying k and α.

In order to neither bore or frighten the reader we refrain from displaying the solutions for the remaining velocity field functions because of their sheer volume. Instead we will display the nonlinear systems, plot the solutions against y and attach them to the Appendix. At $O(\delta^3 A^3 \cos(kz))$ we discover that the nonlinear system depends on F_2 and our solutions are different for each case

$$(\frac{d^2}{dy^2} - k^2)u_{31} = \frac{1}{2}\Big(\frac{u_1v_2'}{2} + 2v_1'u_2 + v_2u_1' + v_1u_2'\Big) + v_{31} + v_1u_M', \tag{2.3.11}$$

$$(\frac{d^2}{dy^2} - k^2)^2v_{31} = \frac{1}{4}\Big(2v_1'v_2'' - v_2v_1''' - v_1''v_2' + v_1v_2'''\Big) - \frac{k^2}{2}(\frac{3}{2}v_1v_2' + 3v_2v_1'), \tag{2.3.12}$$

$$w_{31} = -\frac{1}{k}v_{31}'. \tag{2.3.13}$$

$$\tag{2.3.14}$$

In figure 2.3 we display the undulation functions which adhere to the aforementioned boundary conditions. Finally, our long awaited $O(\delta^3 A'(t))$ system is fairly simple because

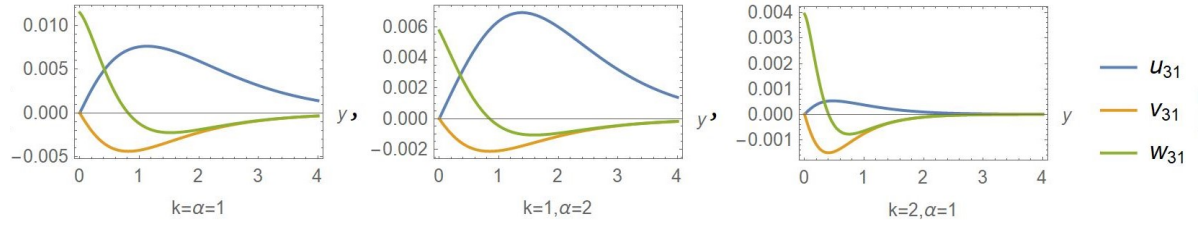

Figure 2.3: $O(\delta^3 A^3 \cos(kz))$ wavy wall velocity field for varying k and α.

of its exclusive dependence on the linear terms due to the trick (2.2.2)

$$(\frac{d^2}{dy^2} - k^2)u_{33} = v_{33} + u_1, \tag{2.3.15}$$

$$(\frac{d^2}{dy^2} - k^2)^2 v_{33} = (\frac{d^2}{dy^2} - k^2)v_1, \tag{2.3.16}$$

$$w_{33} = -\frac{1}{3k}v'_{33}. \tag{2.3.17}$$

In figure 2.4 we exhibit our findings for a deeper understanding.

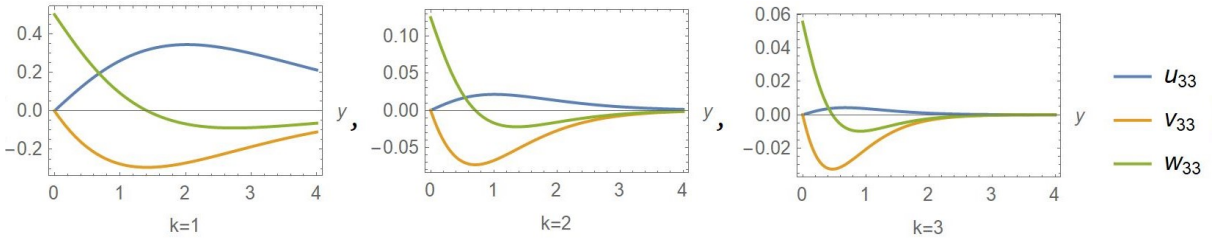

Figure 2.4: $O(\delta^3 A')$ velocity field for varying k.

2.4 Wave Pressure Equation

From section 2.1 we know the wave pressure equation for both cases. In order to proceed we also have to expand the wall shear λ which is dependent on the derivative of the x component at the wall as seen in the aforementioned section. It can be written as

$$\begin{aligned}\lambda = \hat{u}_y(0,z) =& 1 + u_y(0,z) \\ = 1 + \delta\lambda_1\cos(kz) + \delta^2\lambda_2\cos(2kz) &+ \delta^2\lambda_M + \delta^3\lambda_{31}\cos(kz) + \delta^3\lambda_{33}\cos(kz) + \dots.\end{aligned} \tag{2.4.1}$$

Our λ components are then $\lambda_1 = A(t)u'_1(0)$, $\lambda_2 = A(t)^2u'_2(0)$, $\lambda_M = A(t)^2u'_M(0)$, $\lambda_{31} = A(t)^3u'_{31}(0)$ and $\lambda_{33} = A(t)^3u'_{33}(0)$ for simplicity.

2.4.1 Wall Undulation

We set $\Gamma = \Gamma_0(1 + \delta^2\hat{\Gamma})$ with Γ_0 being the linear neutral value of Γ and alter the wave pressure like so for simplifications to occur.

$$P(z) = \rho_1 Q(z) = 3\Gamma_o(ia)^{5/3}Ai'(\xi_0)Q(z). \tag{2.4.2}$$

Inserting the scaled wave pressure into (2.1.21) we acquire

$$Q'' - a^2Q = \lambda^{5/3}(1 + \delta^2\hat{\Gamma}) + \frac{3}{2}\frac{\lambda'}{\lambda}Q'. \tag{2.4.3}$$

We expand the scaled wave pressure Q in true nonlinear stability fashion

$$Q = Q_0 + \delta Q_1\cos(kz) + \delta^2 Q_2\cos(2kz) + \delta^2 Q_M + \delta^3 Q_3\cos(kz), \tag{2.4.4}$$

and manipulate the RHS with the binomial expansion and series identities like so

$$\begin{aligned}\lambda^{5/3} = 1 + \frac{5}{3}\delta\lambda_1\cos(kz) + \frac{5}{3}\delta^2\lambda_2\cos(2kz) + \frac{5}{9}\delta^2\lambda_1^2\cos(kz) \\ + \frac{10}{9}\delta^3\lambda_1\lambda_2\cos(kz)\cos(2kz) + \frac{5}{3}\delta^3\lambda_3\cos(kz) - \frac{10}{81}\delta^3\lambda_1^3,\end{aligned} \tag{2.4.5}$$

$$\frac{\lambda'}{\lambda} = k\Big(- \delta\lambda_1\sin(kz) + \frac{1}{2}\delta^2\sin(2kz)(\lambda_1^2 - 4\lambda_2) + \frac{3}{2}\delta^3\lambda_1\lambda_2\sin(kz)\Big). \tag{2.4.6}$$

Once again, taking orders of 1, δ, δ^2 and δ^3 we retrieve the α, k and $\hat{\Gamma}$ dependent polynomials Q.

$$Q_0 = -a^{-2}, \tag{2.4.7}$$

$$Q_1 = -\frac{5\lambda_1}{2(k^2+a^2)}, \tag{2.4.8}$$

$$Q_2 = -\frac{-10(\lambda_1^2 + 6\lambda_2) + 27k^2\lambda_1 Q_1}{36(a^2+4k^2)}, \tag{2.4.9}$$

$$Q_m = -\frac{36\hat{\Gamma} + 10\lambda_1^2 + 60\lambda_M + 27k^2\lambda_1 Q_1}{36\alpha^2}. \tag{2.4.10}$$

The bold reader can find Q_3 attached in the Appendix.

2.4.2 Transpiration

We repeat the same steps as in the Wall Undulation section. The differences between the two are solely the right hand sides of (2.1.22) and (2.1.21) which lead us into setting the wave pressure as

$$P = \rho_2 Q(z) = -ia\Lambda_0 Q(z), \tag{2.4.11}$$

with $\Lambda = \Lambda_0(1 + \delta^2\hat{\Gamma})$ and Λ_0 its linear neutral value which will ultimately allow us to plot the linear neutral curve. By doing so we simplify our new equation

$$Q'' - a^2 Q = \lambda(1 + \delta\hat{\Gamma}) + \frac{3}{2}\frac{\lambda'}{\lambda}Q'. \tag{2.4.12}$$

We realize that our Q expansion is the same and our RHS is a slightly easier version of (2.4.3). Taking advantage of (2.4.6) and repeating the same method we achieve

$$Q_0 = -a^{-2}, \tag{2.4.13}$$

$$Q_1 = -\frac{\lambda_1}{a^2+k^2}, \tag{2.4.14}$$

$$Q_M = -\frac{4(\lambda_M + \hat{\Lambda}) + 3k^2\lambda_1 Q_1}{4\alpha^2}, \tag{2.4.15}$$

$$Q_2 = -\frac{-4\lambda_2 + 3k^2\lambda_1 Q_1}{4(\alpha^2+4k^2)}, \tag{2.4.16}$$

with Q_3 attached in the Appendix once more.

2.5 Condition at the Wall

We can finally tackle the boundary condition (2.1.18). We multiply both sides of our equation by $-3\lambda^2$ and proceed by manipulating the RHS like so.

$$\begin{aligned}\frac{d}{d\theta}\Big[|\rho Q|^2+\alpha^{-2}|\frac{d(\rho Q)}{d\theta}|^2\Big] &= \frac{d}{d\theta}\Big[\rho\bar{\rho}Q^2+\alpha^{-2}\rho\bar{\rho}(\frac{dQ}{d\theta})^2\Big] \\ = \frac{d}{d\theta}\Big[|\rho|^2Q^2+\alpha^{-2}|\rho|^2(\frac{dQ}{d\theta})^2\Big] &= 2|\rho^2|\frac{dQ}{d\theta}\Big[Q+a^{-2}(\frac{d^2Q}{d\theta^2})\Big],\end{aligned} \tag{2.5.1}$$

with ρ the respective wave pressure scaling variable $P=\rho Q$.

2.5.1 Wall Undulation

For the wall undulation case at $O(\delta)$ we obtain

$$\rho_1 = \frac{A(\tau)w_1(0)}{2kQ_0Q_1} = \frac{6}{,}5a^2(a^2+k^2) \tag{2.5.2}$$

which in turn delivers us the linear neutral value that agrees with the findings in Hall, 2022.

$$\Gamma_0^2 = \frac{2(\alpha^2+k^2)}{5\alpha^{4/3}|Ai'(0)|^2}. \tag{2.5.3}$$

Our linear neutral curves can be seen in figure 2.5 from which we realize that instability

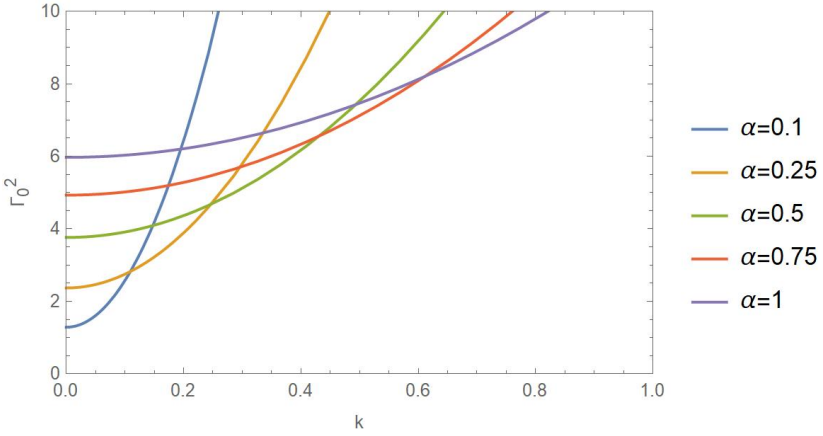

Figure 2.5: Γ_0^2 Neutral Curve.

occurs at $k=0$. Next up at $O(\delta^2)$ we uncover the F_2 polynomial in terms of a and k

$$F_2 = \frac{-11\alpha^4-8\alpha^2k^2+243k^4}{288k^2(\alpha^2+k^2)}, \tag{2.5.4}$$

which allowed us to plot the F_2 dependent velocity field solutions in section 2.3. It is evident that our long awaited amplitude ODE will appear at $O(\delta^3)$ since the amplitude itself alongside its derivative cancels out in the previous two orders. The familiar structure

of the ODE is depicted below

$$A'(\tau) = \frac{8\hat{\Gamma}k^2}{3}A(\tau) + \frac{\left(242\alpha^6 - 2401\alpha^4k^2 - 11100\alpha^2k^4 + 183k^6\right)}{82944k^2(\alpha^2+k^2)^2}A(\tau)|A(\tau)|^2. \quad (2.5.5)$$

The Stuart-Landau equation that appears was discussed in section 1.3 from which we will make our assumptions. We could continue by plotting the $A(\tau)^3$ coefficient as a function of two variables α and k but that would simply overcomplicate matters We firstly set $\gamma_1 = \alpha/k$ and the undulation coefficient (UC) becomes

$$UC = \frac{(242\gamma_1^6 - 2401\gamma_1^4 - 11100\gamma_1^2 + 183)}{82944(\gamma_1^2+1)^2} \quad (2.5.6)$$

and proceed to plot the $A(\tau)^3$ coefficient in figure 2.6 in order to understand the nature of our flow From it we understand that there are two present sign changes at approximately

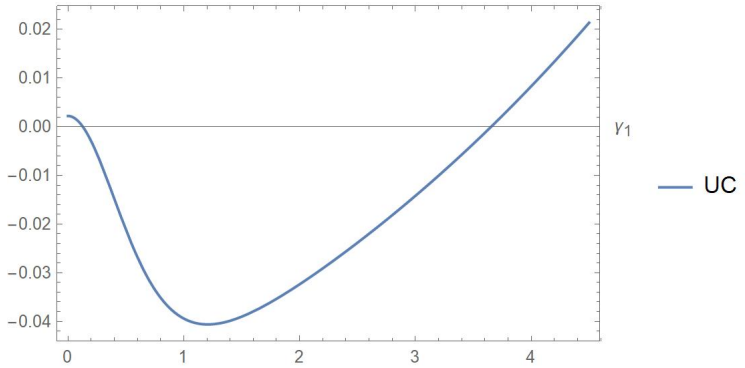

Figure 2.6: Undulation $A^3(\tau)$ coefficient.

$\gamma_1 = 0.128$ and $\gamma_1 = 3.654$. Therefore, our flow is momentarily supercritical prior to $\gamma_1 = 0.128$, subcritical between the two roots and supercritical following $\gamma_1 = 3.654$. We are of course interested in the laminar flow case so this is a positive outcome which indicates a further insight to the linear stability theory in Hall, 2022 which was based solely on the Γ_0^2 neutral curves which can be seen in figure 2.5.

2.5.2 Transpiration

Replicating our work for the transpiration case we collect the terms of the leading $O(\delta)$ and attain

$$\rho_2^2 = \frac{3A(\tau)w_1(0)}{2kQ_0Q_1} = 6\alpha^2(\alpha^2+k^2) \Rightarrow \quad (2.5.7)$$

$$\Lambda_0^2 = 6(\alpha^2+k^2). \quad (2.5.8)$$

This allows us to plot our neutral curve Λ_0^2 and we realize that once again instability occurs as $k \to 0$. In order to further analyze the character of our flow we recover F_2

$$F_2 = \frac{7\alpha^4 + 24\alpha^2k^2 + 65k^4}{96k^2(\alpha^2+k^2)}, \quad (2.5.9)$$

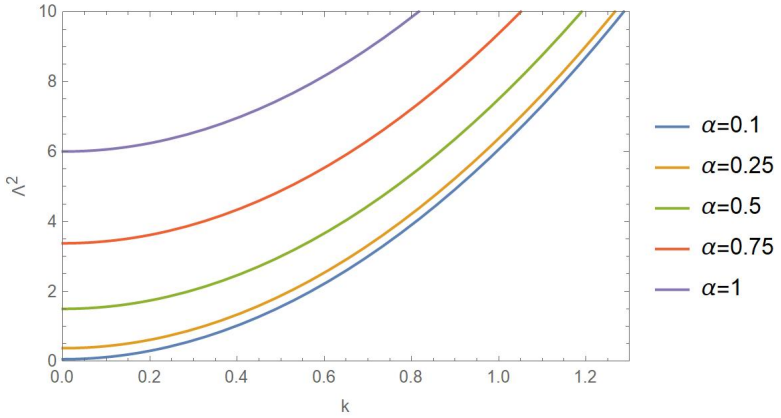

Figure 2.7: Λ_0^2 neutral curve.

and proceed to the well awaited *Stuart-Landau* equation which is

$$A'(\tau) = \frac{8\hat{\Lambda}k^2}{3}A(\tau) - \frac{(14\alpha^6 + 297\alpha^4k^2 + 652\alpha^2k^4 - 207k^6)}{9216k^2(\alpha^2 + k^2)^2}A(\tau)|A(\tau)|^2. \tag{2.5.10}$$

We realize that both the wall undulation and transpiration $A(\tau)$ coefficients have the same structure but unfortunately do not contribute into the characterisation of the type of flow that we have. We set

$$\gamma_2 = \frac{\alpha}{k}, \tag{2.5.11}$$

making our transpiration coefficient (TC) to be

$$TC = -\frac{(14\gamma_2^6 + 297\gamma_2^4 + 652\gamma_2^2 - 207)}{9216(\gamma_2^2 + 1)^2}. \tag{2.5.12}$$

In figure 2.8 we discern that TC starts off being positive from 0.022 and crosses the γ_2 axis at approximately $\gamma_2 = 0.53$. Thus, the flow is supercritical prior to and subcritical after the single root. This result acts as an addition to the linear stability theory undertaken

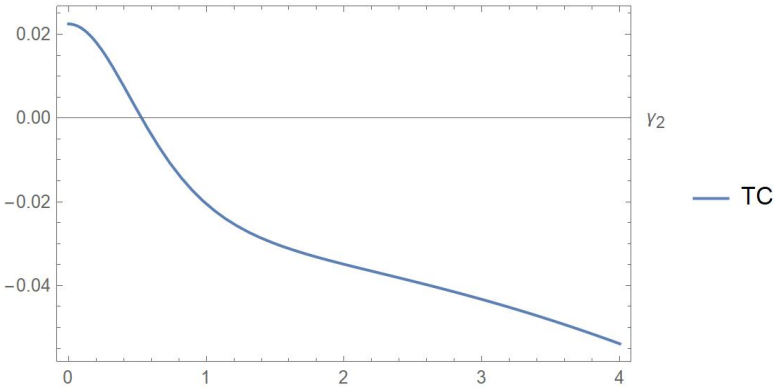

Figure 2.8: Transpiration $A^3(\tau)$ coefficient.

in Hall, 2022 which was based only on the Λ_0^2 neutral curves that we acquired in figure 2.8.

Chapter 3

Pipe Case

We now proceed to work on the more advanced topic of pipe flow and thus will be solving the continuity equation

$$\nabla \cdot \hat{\mathbf{u}} = \frac{1}{r}\frac{\partial(r\hat{u})}{\partial r} + \frac{1}{r}\frac{\partial \hat{v}}{\partial \theta} + \frac{\partial \hat{w}}{\partial z} = 0, \tag{3.0.1}$$

alongside the *Cylindrical Navier-Stokes*

$$\big(\frac{\partial \hat{u}}{\partial t} + \hat{u}\frac{\partial \hat{u}}{\partial r} + \frac{\hat{v}}{r}\frac{\partial \hat{u}}{\partial \theta} + \hat{w}\frac{\partial \hat{u}}{\partial z} - \frac{\hat{w}^2}{r}\big) = -\frac{\partial \hat{p}}{\partial r} + \frac{1}{Re}\big(\nabla^2\hat{u} - \frac{\hat{u}}{r^2} - \frac{2}{r^2}\frac{\partial \hat{v}}{\partial \theta}\big), \tag{3.0.2}$$

$$\big(\frac{\partial \hat{v}}{\partial t} + \hat{u}\frac{\partial \hat{v}}{\partial r} + \frac{\hat{v}}{r}\frac{\partial \hat{v}}{\partial \theta} + \hat{w}\frac{\partial \hat{v}}{\partial z} + \frac{\hat{u}\hat{v}}{r}\big) = -\frac{1}{r}\frac{\partial \hat{p}}{\partial \theta} + \frac{1}{Re}\big(\nabla^2\hat{v} - \frac{\hat{v}}{r^2} + \frac{2}{r^2}\frac{\partial \hat{u}}{\partial \theta}\big), \tag{3.0.3}$$

$$\big(\frac{\partial \hat{w}}{\partial t} + \hat{u}\frac{\partial \hat{w}}{\partial r} + \frac{\hat{v}}{r}\frac{\partial \hat{w}}{\partial \theta} + \frac{\hat{v}}{r}\frac{\partial \hat{w}}{\partial \theta} + \hat{w}\frac{\partial \hat{w}}{\partial z}\big) = -\frac{\partial \hat{p}}{\partial z} + \frac{1}{Re}\nabla^2\hat{w}, \tag{3.0.4}$$

with the Cylindrical Laplacian being

$$\nabla^2 = \frac{1}{r}\frac{\partial}{\partial r} + \frac{1}{r^2}\frac{\partial^2}{\partial \theta^2} + \frac{\partial^2}{\partial z^2}. \tag{3.0.5}$$

The $\hat{u}, \hat{v}$ and $\hat{w}$ are the radial, azimuthal and streamwise velocity components respectively whilst Re is the Reynolds number and $\hat{p}$ is the pressure.

3.1 VWI Equations

We presume that our shear flow is driven by a fixed streamwise gradient pressure $p = -\frac{4z}{Re}$ resulting into a *Hagen-Poiseuille* flow with $w_0 = 1 - r^2$. We will soon induce a perturbation to our flow taking the limits $\epsilon \to 0, R \to \infty$ and assuming that $\epsilon R^{1/3} \ll 1$ and $\alpha = O(1)$. Smith, 1982 realized that the wall amplitude is small compared to the thickness of the viscous wall layer in this case. Following the nonlinear stability theory from Chapter 1 we introduce the wavy wall as $r = 1 + \epsilon\cos(E + \bar{E})$ and our perturbations

$$\begin{aligned} \hat{\mathbf{u}} = (0, 0, w_0(r)) + \Big(\frac{u(r,\theta)}{Re}, \frac{v(r,\theta)}{Re}, w(r,\theta)\Big), \\ \hat{p} = -\frac{4z}{Re} + \frac{p(r,\theta)}{Re^2}. \end{aligned} \tag{3.1.1}$$

This assumption results into our new system of equations which is the equivalent of the plane case with minor alterations

$$\frac{\partial(ru)}{\partial r}+\frac{\partial v}{\partial \theta}=0, \tag{3.1.2}$$

$$u\frac{\partial u}{\partial r}+\frac{v}{r}\frac{\partial u}{\partial \theta}-\frac{v^2}{r}=-\frac{\partial p}{\partial r}+\nabla^2 u-\frac{u}{r^2}-\frac{2}{r^2}\frac{\partial v}{\partial \theta}, \tag{3.1.3}$$

$$u\frac{\partial v}{\partial r}+\frac{v}{r}\frac{\partial v}{\partial \theta}+\frac{uv}{r}=-\frac{1}{r}\frac{\partial p}{\partial \theta}+\nabla^2 v-\frac{v}{r^2}+\frac{2}{r^2}\frac{\partial u}{\partial \theta}, \tag{3.1.4}$$

$$u\frac{\partial w}{\partial r}+\frac{v}{r}\frac{\partial w}{\partial \theta}=\nabla^2 w+4, \tag{3.1.5}$$

and a regularity boundary condition at $r=0$. The wave pressure equation that we acquired from the wall layer in Hall, 2022 and our working from the plane case holds true for the cylindrical coordinates. The wave pressure is now dependent on θ, the streamwise component of our flow is W, the wall shear λ is replaced by μ, σ by $\Delta=-i\alpha\mu$ with α being our wavelength.

$$\frac{d^2P}{d\theta^2}-\frac{3}{2}\frac{\mu'}{\mu}\frac{dP}{d\theta}-a^2P=-a\omega W_0-3i\alpha\Delta^{2/3}Ai'(\xi_0)W_0-\Delta V_0. \tag{3.1.6}$$

We know that $W_0=-\mu\Gamma$ and $V_0=0$ and take the simpler case $\omega=0$ which in turn causes $\xi_0=0$.Also, $\Gamma=\Gamma_0(1+\hat{\Gamma}\delta^2)$, where Γ_0 is our linear neutral value, transforms the ODE into the familiar

$$\frac{d^2P}{d\theta^2}-\frac{3}{2}\frac{\mu'}{\mu}\frac{dP}{d\theta}-a^2P=-3(i\alpha)^{5/3}Ai'(0)\Gamma_0(-\mu)^{5/3}(1+\hat{\Gamma}\delta^2)=\rho_3(-\mu)^{5/3}(1+\hat{\Gamma}\delta^2), \tag{3.1.7}$$

where $\rho_3=-3(i\alpha)^{5/3}Ai'(0)\Gamma_0$.

3.2 Expansions and Final System

Having introduced our system of equations we can now continue onto our respective nonlinear stability expansions. Unlike the plane case all our trigonometric functions are in terms of θ instead of y with M being the analogous spanwise wavenumber instead of k. We proceed with even θ streamwise and radial velocity components whilst the alternative odd case alongside more extensive background can be found in Hall and Ozcakir, 2021.

$$\begin{aligned}\mathbf{u}(r,\theta)=&\delta A(\tau)\big[u_1(r)\cos(M\theta),v_1(r)\sin(M\theta),w_1(r)\cos(M\theta)\big]\\&+\delta^2A^2(\tau)\big[0,0,w_M(r)\big]\\&+\delta^2A^2(\tau)\big[u_2(r)\cos(2M\theta),v_2(r)\sin(2M\theta),w_2(r)\cos(2M\theta)\big]\\&+\delta^3A^3(\tau)\big[u_{31}(r)\cos(M\theta),v_{31}(r)\sin(M\theta),w_{31}(r)\cos(M\theta)\big]\\&+\delta^3A^3(\tau)\big[u_{32}(r)\cos(3M\theta),v_{32}(r)\sin(3M\theta),w_{32}(r)\cos(3M\theta)\big]\\&+\delta^3A'(\tau)\big[u_{33}(r)\cos(M\theta),v_{33}(r)\sin(M\theta),w_{33}(r)\cos(M\theta)\big],\end{aligned} \tag{3.2.1}$$

$$\begin{aligned}p(r,\theta)=&\,\delta A(\tau)p_1(r)\cos(M\theta)+\delta^2A^2(\tau)p_M(r)+\delta^2A^2(\tau)p_2(r)\cos(2M\theta)\\&+\delta^3A^3p_{31}(r)\cos(M\theta)+\delta^3A^3p_{32}(r)\cos(3M\theta)+\delta^3A'(\tau)p_{33}(r)\cos(M\theta).\end{aligned} \tag{3.2.2}$$

Where we have set $\tau = \delta^2 t$ for simplicity purposes which will become clear soon. The $w_M(r)$ and p_M velocity field functions are the mean flow corrections which arise from the Reynolds stresses whilst the harmonic terms at $O(\delta^3 A^3(t)\cos(3kz))$ will be ignored and the $O(\delta^3 A'(t))$ will allow us to acquire the Stuart-Landau Equation when solving the condition at the wall for the azimuthal component of our velocity field. Additionally, we have set the streamwise and axial velocity components of our vortex to be even functions of θ unlike the azimuthal velocity component which is odd because of the rolls of our nonlinear system.

The insertion of these nonlinear expansions into the system of equations would presently wreak havoc so instead, a simplification of the so called system will be undertaken. Firstly we multiply (3.1.4) by $(-r)$ and differentiate it by ∂r. We continue by differentiating (3.1.3) by $\partial\theta$ and add the altered (3.1.3) and (3.1.4) equations to rid our selves of the pressure. Taking advantage of the continuity equation (3.2.6) we can subsequently derive a PDE in terms of $u(r,\theta)$ which will then be transformed into an ODE with the aforementioned expansions (3.2.1). We know that our Amplitude is constant on the neutral curve and becomes

$$\frac{dA}{dt} = \delta^2 \frac{dA}{d\tau} = \delta^2 A'(\tau) = 0, \tag{3.2.3}$$

with the help of $\tau = \delta^2 t$. The purpose of which revolves around the isolation of $A'(\tau)$ in the $O(\delta^3)$ terms for simplicity and clarity for the reader. Before presenting the two newly found equations one has to point out that normal differentiation rules and identities can be manipulated to our advantage because our expansions $\mathbf{u}(r,\theta)$ are separable.Thus, we acquire

$$\frac{\partial}{\partial r}\Big[(r\nabla^2 - \frac{1}{r} - \frac{\partial}{\partial\tau})(\frac{\partial(ru)}{\partial r})\Big] + (\nabla^2 + \frac{3}{r^2})\frac{\partial^2 u}{\partial\theta^2} = \frac{\partial^2 J_1}{\partial^2\theta} - \frac{\partial}{\partial r}(r\frac{\partial J_2}{\partial\theta}), \tag{3.2.4}$$

$$(\nabla^2 - \frac{\partial}{\partial\tau})w = J_3 - 2ru, \tag{3.2.5}$$

$$\frac{\partial(ru)}{\partial r} + \frac{\partial v}{\partial\theta} = 0, \tag{3.2.6}$$

with the regularity condition at the centre of the pipe and the wall condition being

$$\mathbf{u} = (0, 0, -\frac{1}{3}(\frac{1}{\mu^2}\frac{\partial}{\partial z}[|P|^2 + \alpha^{-2}|P_z|^2])) \quad \text{at} \quad y = 0. \tag{3.2.7}$$

The mentioned J terms that constitute the RHS of our system are

$$\begin{aligned} J_1 &= u\frac{\partial u}{\partial r} + \frac{v}{r}\frac{\partial u}{\partial\theta} - \frac{v^2}{r}, \\ J_2 &= u\frac{\partial v}{\partial r} + \frac{v}{r}\frac{\partial v}{\partial\theta} + \frac{uv}{r}, \\ J_3 &= u\frac{\partial w}{\partial r} + \frac{v}{r}\frac{\partial w}{\partial\theta}. \end{aligned} \tag{3.2.8}$$

3.3 Velocity Field Terms

Inserting the expansions into our newly acquired nonlinear system of equations we amass the different ordered terms separately . The main theme of this chapter is the prominent linear LHS of the analogous equations and their constantly changing nonlinear RHS's which depend on the previous orders resulting into increasingly more complicated polynomials in terms of M which will be part of our solutions. We unveil the u_i terms first with $i = 1, 2, M, 31, 33$ neglecting the constants that accompany their negative r powers because of the regularity at the pipe and unveiling one of the constants that accompanies a positive r powered term with the *no-slip* condition. The general solution is

$$u_i = u_h + u_p = c_1 r^{-\bar{M}+1} + c_2 r^{-\bar{M}-1} + c_3 r^{\bar{M}+1} + c_4 r^{\bar{M}-1} + u_p, \tag{3.3.1}$$

where u_p contains positive powers of r and polynomials in terms of $\bar{M}$ where $\bar{M} = 1M, 2M$ or$3M$. Through (3.2.6) we discover the azimuthal part of our velocity field and finally the streamwise component which takes the form

$$w_i = w_h + w_p = \frac{1}{2} r^{-\bar{M}}(c_1(1 + r^{2\bar{M}}) + ic_2(-1 + r^{2\bar{M}}))) + w_p. \tag{3.3.2}$$

Here, w_p is alike u_p and we continue by reapplying the regularity condition at the centre of the pipe and no slip at the wall. One constant L_k with $k = 1, 2, 31, 33$ will be left throughout these orders and will be able to merge L_{31} and L_{33} later because of the mutual linear part of the $O(\delta^3 A')$ and $O(\delta^3 A^3)$ velocity field functions. Thus, collecting all the $O(\delta)$ terms we solve the linear system that can also be found in Hall and Ozcakir, 2021

$$\begin{aligned} \frac{\partial}{\partial r}\big[(r\nabla^2 - \frac{1}{r})(\frac{\partial(ru_1\cos(M\theta))}{\partial r})\big] + (\nabla^2 + \frac{3}{r^2})\frac{\partial^2 u_1\cos(M\theta)}{\partial\theta^2} &= 0, \\ \nabla^2 w_1\cos(M\theta) &= -2ru_1\cos(M\theta), \\ \frac{\partial(ru_1\cos(M\theta))}{\partial r} + \frac{\partial(v_1\sin(M\theta))}{\partial\theta} &= 0, \end{aligned} \tag{3.3.3}$$

resulting into

$$\mathbf{u}_1 = L1\Big(r^{M-1} - r^{M+1}, r^{M-1}\frac{r^2(2+M) - M}{M}, \frac{r^M}{4}(r^2-1)(\frac{-2}{1+M} + \frac{1+r^2}{2+M})\Big). \tag{3.3.4}$$

The additional normalization condition $w_1'(1) = 0$ only takes place here for further simplification and allows us to obtain $L_1 = -(M+1)(M+2)$ .We plot our solutions in figure 3.1 where it can be seen that the linear velocity components comply to the boundary conditions.

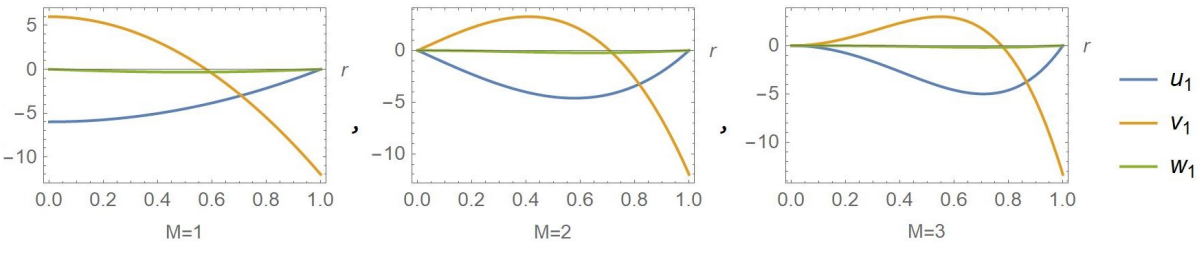

Figure 3.1: Linear Velocity functions for varying M.

Continuing in similar fashion we collect the $O(\delta^2)$ mean flow terms which can only be found in the streamwise equation (3.2.5) because of the prominent mean flow correction w_M within our streamwise expansion and the nonlinear Q_3 term.Additionally, we collect all the $O(\delta^2 \cos 2M\theta)$ which are independent of the mean flow terms and find the overall system for the second order to be

$$\nabla^2 w_M = \frac{1}{2r}(-Mv_1w_1 + ru_1w_1'), \tag{3.3.5}$$

$$\begin{aligned}\frac{\partial}{\partial r}\big[(r\nabla^2 - \frac{1}{r})(\frac{\partial(ru_2\cos(2M\theta))}{\partial r})\big] + (\nabla^2 + \frac{3}{r^2})\frac{\partial^2 u_2\cos(2M\theta)}{\partial\theta^2} = \\ -\frac{1}{r}M\cos(2M\theta)\Big(u_1\big((r^2v_1' - rv_1)' - 2Mu_1\big) - (r^2u_1v_1)'\Big),\end{aligned} \tag{3.3.6}$$

$$\nabla w_2\cos(2M\theta) = \frac{1}{2r}\cos(2M\theta)\big(-4r^2u_2 + ru_1w_1' - (ru_1)'w_1\big), \tag{3.3.7}$$

$$\frac{\partial(ru_2)}{\partial r} + 2Mv_2 = 0. \tag{3.3.8}$$

We will refrain from displaying the second and third order components of our velocity field. Instead we will plot them for varying M, a in figure 3.2 and will attach only the second ordered functions in the Appendix. The constant L_2 that we have collected from this order will be unveiled while solving the wall condition and is in terms of α and M.

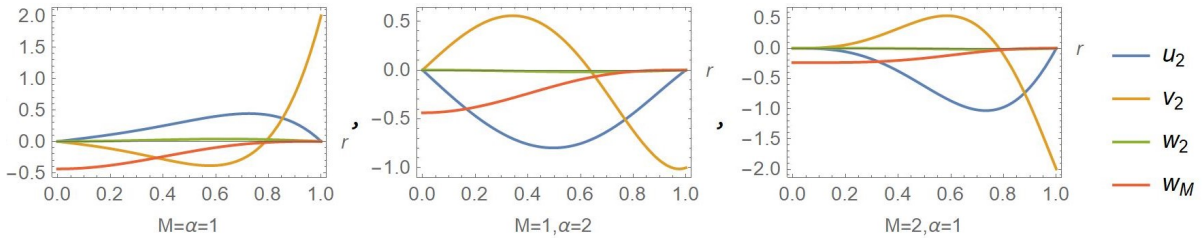

Figure 3.2: Second Order Velocity functions for varying M and α.

It is important to note that the $O(\delta^3 A')$ ODE system is dependent only on the linear velocity field functions because of the presence of $\frac{\partial}{\partial t} = \delta^2\frac{\partial}{\partial\tau}$ and could be solved prior to the second order but in return the nonlinear terms are much more complicated. The system is as follows

$$\begin{aligned}\frac{\partial}{\partial r}\big[(r\nabla^2 - \frac{1}{r})(\frac{\partial(ru_{33}\cos(M\theta)}{\partial r})\big] + (\nabla^2 + \frac{3}{r^2})\frac{\partial^2 u_{33}\cos(M\theta)}{\partial\theta^2} = \\ (\frac{\partial^2}{\partial r^2}r - M^2)(u_1\cos(M\theta)),\end{aligned} \tag{3.3.9}$$

$$\nabla^2 w_{33}\cos(M\theta) = w_1\cos(M\theta), \tag{3.3.10}$$

$$\frac{\partial(ru_{33}\cos(M\theta))}{\partial r}+\frac{\partial(w_{33}\sin(M\theta))}{\partial\theta}=0, \tag{3.3.11}$$

and our plots when $L_{33}=0$ are

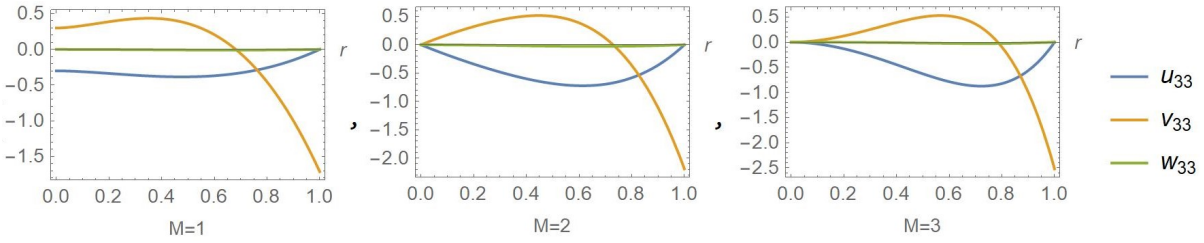

Figure 3.3: $\mathbf{U}_{33}$ Velocity functions for varying M and α.

Next up, the $O(\delta^3A^3)$ system of equations is

$$\frac{\partial}{\partial r}\Big[(r\nabla^2-\frac{1}{r})(\frac{\partial(ru_{33}\cos(M\theta))}{\partial r})\Big]+(\nabla^2+\frac{3}{r^2})\frac{\partial^2u_{33}\cos(M\theta)}{\partial\theta^2}= \frac{\partial^2(ru_1\cos(M\theta))}{\partial r^2}-M^2u_1\cos(M\theta), \tag{3.3.12}$$

$$\frac{\partial(ru_{31}\cos(M\theta))}{\partial r}+\frac{\partial v_{31}\sin(M\theta)}{\partial\theta}=0, \tag{3.3.13}$$

$$\nabla^2w_{31}\cos(M\theta)= \tag{3.3.14}$$

$$\frac{\cos(M\theta)}{2r}\Big[-M(v_2w_1+2v_1w_2)+r(-4ru_{31}+u_2w_1'+u_1(w_2'+2w_M))\Big], \tag{3.3.15}$$

with our terms being dependent on L_2 and hence α. For $L_{31}=0$ the nature of our velocity field at this order is

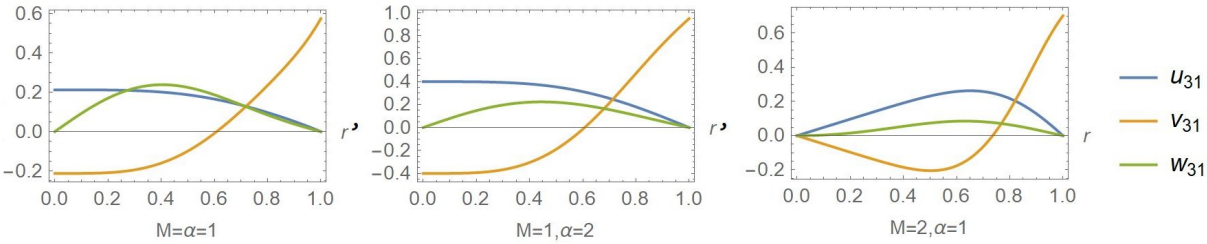

Figure 3.4: $\mathbf{u}_{31}$ Velocity functions for varying M and α.

Finally, whilst we do not display the functions explicitly here it is important to note that

$$(L_{31}+L_{33})\mathbf{u}_L+\mathbf{u}_{31N}+\mathbf{u}_{33N}=2L_3\mathbf{u}_L+\mathbf{u}_{31N}+\mathbf{u}_{33N},$$

because the linear parts of $\mathbf{u}_{31}$ and $\mathbf{u}_{33}$ are the same and setting $L_{31}=L_{33}=L_3$ we merge our constants for further simplification in the coming chapters.

3.4 Wave Pressure Equation

We know from 3.1 that $P = \rho_2 Q$ and expand our wave pressure Q and wall shear μ like so

$$Q = Q_0 + \delta Q_1 \cos(M\theta) + \delta^2(Q_2 \cos(2M\theta) + Q_M) + \delta^3 Q_3 \cos(M\theta), \tag{3.4.1}$$

$$\mu = \mu_0 + \delta\mu_1 c_1 + \delta^2\big(\mu_2 \cos(2M\theta) + \mu_M\big) + \delta^3\big(\cos(M\theta)(\mu_{31} + \mu_{33}) + \cos(3M\theta)\mu_{32}\big). \tag{3.4.2}$$

The Q_M and μ_M terms are the mean flow corrections that arise from the Reynolds stresses and our μ terms are

$$\begin{aligned} &\mu_0 = w_0'(1) = -2, \mu_1 = A(\tau)w_1'(1), \mu_2 = A(\tau)^2 w_2'(1), \mu_M = A(\tau)^2 W_M'(1), \\ &\mu_{31} = A(\tau)^3 w_{31}'(1), \mu_{32} = A(\tau)^3 w_{32}'(1), \mu_{33} = A'(\tau)^3 w_{33}'(1). \end{aligned} \tag{3.4.3}$$

As we will see the μ_{32} term does not play an active role so we will tend to ignore it. After the eminent substitution and further simplification our new wave pressure equation is

$$\frac{d^2Q}{d\theta^2} - \alpha^2 Q = (-\mu)^{5/3}(1 + \hat{\Gamma}\delta^2) + \frac{3}{2}\frac{\mu'}{\mu}\frac{dQ}{d\theta}. \tag{3.4.4}$$

One realizes the likeness between the equivalent plane pressure equation (2.4.3) and (3.4.4). We manipulate our RHS like so in order to proceed

$$\frac{\mu'}{\mu} = \mu'\Big[\mu_0 - \delta\mu_1 c_1 + \delta^2(\mu_2 c_2 + \mu_M) - \delta^3 c_1(\mu_{31} + \mu_{33})\Big],$$

$$(-\mu)^{5/3} = (2 + (-\mu - 2))^{5/3} = 2^{5/3} - \frac{5}{3}2^{2/3}(\mu + 2) + \frac{5}{9}2^{-1/3}(\mu + 2)^2 + \frac{5}{81}2^{-4/3}(\mu + 2)^3,$$

by using series identities and the fractional binomial expansion. Before collecting the wanted Q terms it is important to mention that they will be dependent on the amplitude equation as well as a, $\hat{\Gamma}$ and M. Collecting terms of orders $O(1)$, $O(\delta\cos(M\theta))$, $O(\delta^2)$, $O(\delta^2\cos(2M\theta))$, $O(\delta^3\cos(M\theta))$ we find

$$Q_0 = -\frac{2^{5/3}}{\alpha}, \tag{3.4.5}$$

$$Q_1 = \frac{5}{3}2^{2/3}\frac{\mu_1}{(\alpha^2 + M^2)}, \tag{3.4.6}$$

$$Q_M = \frac{2^{2/3}(-72\hat{\Gamma} + 5\mu_1^2 + 60\mu_M) + 54M^2\mu_1 Q_1}{36\alpha^2}, \tag{3.4.7}$$

$$Q_2 = \frac{2^{2/3}(5\mu_1^2 + 60\mu_2) - 54M^2\mu_1 Q_1}{36(\alpha^2 + 4M^2)}, \tag{3.4.8}$$

$$\begin{aligned} Q_3 = &\frac{5\big(144\hat{\Gamma}\mu_1 - \mu_1^3 + 144(\mu_{31} + \mu_{33}) + 24\mu_1(\mu_2 + 2\mu_M)\big)}{2162^{1/3}(\alpha^2 + M^2)} \\ &+ \frac{3M^2\big(\mu_1^2 Q_1 + 8\mu_2 Q_1 + 8\mu_1 Q_2\big)}{8(\alpha^2 + M^2)}. \end{aligned} \tag{3.4.9}$$

It should be mentioned that Q_3 is in terms of $A(t)$, $A(t)^3$ and $\hat{\Gamma}$ a fact which proves to be of importance because of its role in constructing the well wanted Stuart-Landau Equation.

3.5 Azimuthal Condition at the Wall

We finally arrive at the wall condition at $r = 1$ of the azimuthal component which is almost identical to the plane case condition once more

$$v(1) = -\frac{1}{3}\Big(\frac{1}{\mu^2}\frac{d}{d\theta}\Big[|P|^2 + \alpha^{-2}|\frac{dP}{d\theta}|^2\Big]\Big). \tag{3.5.1}$$

Our RHS consists of $O(\delta)$ terms which we manipulate like in 2.5.1 where we have used complex conjugate identities. Repeating the same steps we amass all the $O(\delta)$ as well as $O(\delta^2)$ terms and annex the constants $|\rho|^2$ and L_2 which were collected from the wave pressure and the second order system of our *Navier-Stokes*. The modulus of our constant is thus

$$|\rho|^2 = \frac{6A(\tau)V_1(1)}{MQ_0Q_1} \Rightarrow \Gamma_0 = \frac{(\alpha^2 + M^2)(M+1)(M+2)}{2^{1/3}5M^2\alpha^{4/3}[Ai'(0)]^2}. \tag{3.5.2}$$

Our neutral curves are given by Γ_0 which coincides with the one reached by Hall and Ozcakir, 2021. These neutral curves can be seen in figure 3.5

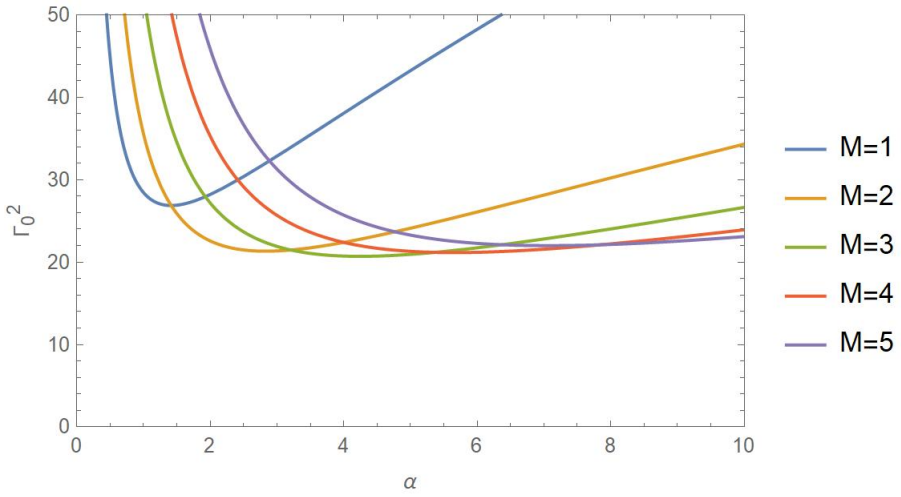

Figure 3.5: Neutral Curves for varying M.

and we realize that the minimum of the Γ_0^2 which is the most dangerous mode is located at $\alpha^2 = 2M^2$ as seen below in figure 3.6. The display of the enormous L_2 constant does not take place but it is important to mention the singularity that arises at

$$\alpha^2 = 2M^3. \tag{3.5.3}$$

This equality carries a lot of importance which we will allude to in the coming order as well as this one. When trying to uncover more details in regards to Γ_0 and its different

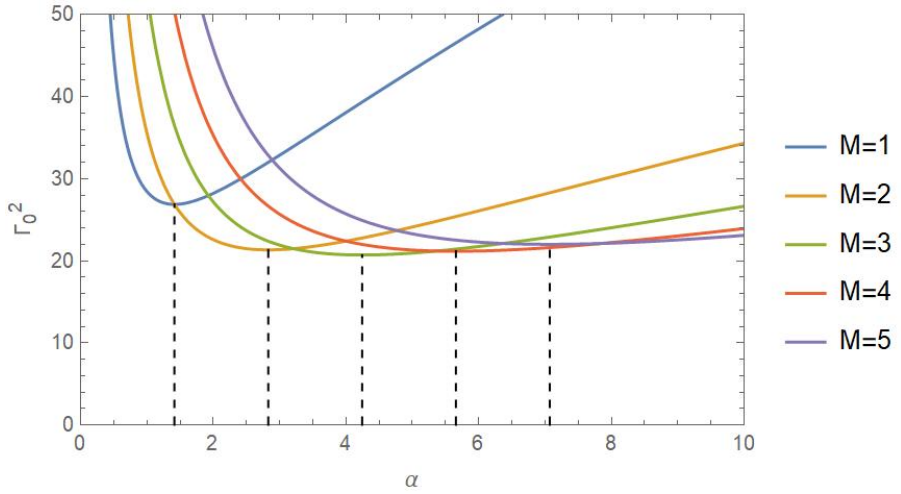

Figure 3.6: Minimum points at $(M\sqrt{2}, \Gamma(\sqrt{2}, M))$.

modes we find that our two most dangerous ones are equal when

$$\Gamma_0(\alpha, M) = \Gamma_0(\alpha, 2M) \Rightarrow \alpha^2 = 2M^3, \tag{3.5.4}$$

So, it is evident that the nature of our flow will possibly change at the $\alpha^2 = 2M^3$ point. Finally, from $O(\delta^3)$ we attain our *Stuart-Landau* equation which takes the form

$$A'(t) = A(t)T_1(\alpha, M, \hat{\Gamma}) + A(t)^3 T_2(\alpha, M). \tag{3.5.5}$$

It is of crucial importance that no free constants from the *Navier-Stokes* or wave pressure equation remain in the $A(t)^3$ coefficient unlike the $A(t)$ coefficient as can be seen above. That is due to the fact that progressing requires us to address the parameters α and M as variables. The singularity from L_2 is carried over and affects the $A(\tau)^3$ coefficient's sign which is crucial as explained in section 1.3. We display the plot of $T_2(\alpha, M)$ in figure 3.7 and can notice some irregularities near $M = 0$ but can not pin point all of them. For

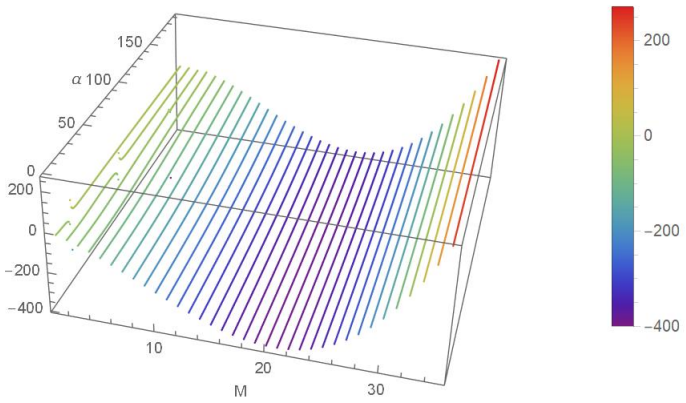

Figure 3.7: 3D Plot of the $A^3(\tau)$ Coefficient.

simplicity we will plot the coefficient again, this time in 2D, with varying α for the reader to realize the possible sign change because of the present singularity.

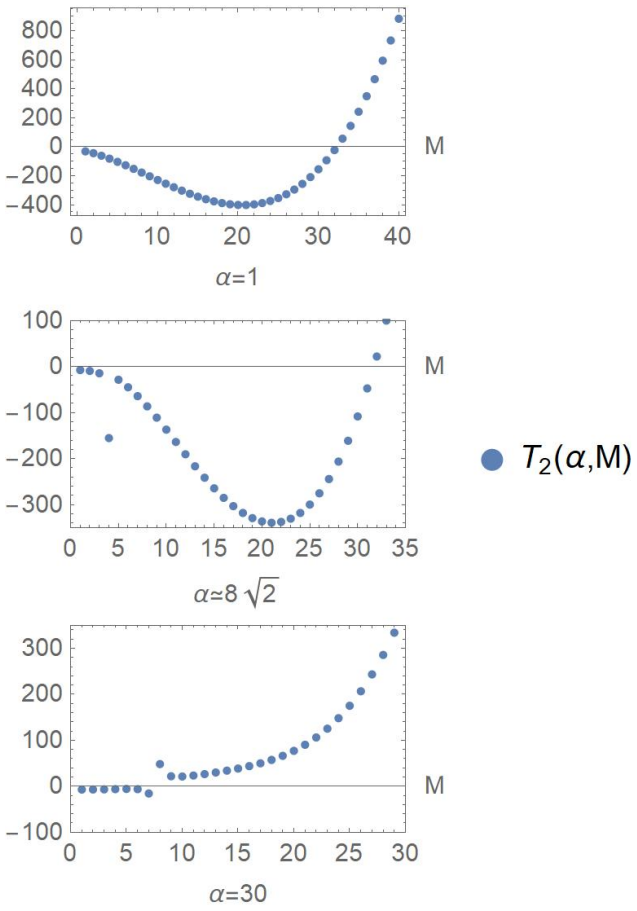

Figure 3.8: 2d Plot of the $A^3(\tau)$ Coefficient.

We notice the jump in value that accompanies our plots in figure 3.8 as α approaches the singularity and we have deliberately plotted the $T_2(\alpha, M)$ coefficient at $\alpha \approx 8\sqrt{2}$ which is a singularity in order to exhibit it. As $k \to 0$ the flow is subcritical and as $k \to \infty$ the flow is supercritical.

Chapter 4

Conclusion

In this report we have considered pipe or channel flows modified by a wavy wall or transpiration applied at the wall. Solutions of the weakly nonlinear stability problem governing the bifurcation of small amplitude solutions near the linear stability neutral curve have been found using a multiple scales asymptotic approach. The approach requires that the flow Reynolds number is large and the amplitude of the wave needed to provoke an instability is asymptotically small in terms of the Reynolds number.

The amplitude of the disturbance bifurcating at the linear stability point satisfies a first order nonlinear differential equation usually referred to as the Stuart Landau equation. It is shown that the coefficient of the cubic term in the amplitude equation can have positive or negative real parts depending on the forcing streamwise wavenumber. When the bifurcation is supercritical the theory predicts that a stable small amplitude solution will bifurcate at the linear stability point. If the bifurcation is subcritical then the small finite amplitude solution exists below the linear stability point and is linearly unstable. In that case a sufficiently large perturbation to the stable steady state will lead to unbounded growth with no stable finite amplitude state being available. The latter is the case for plane Poiseuille flow where it is well-documented how large amplitude disturbances lead to bypass transition.

The instability described here is in the form of streamwise vortices and so is very similar in structure to Taylor-Görtler vortices. However it is well-known that Taylor-Görtler vortices bifurcate supercritically which differs from the case here where both sub and supercritical bifurcations are possible. The analysis given here shows that for certain spanwise (channel) or azimuthal (pipe) wavenumbers a value for the streamwise wavenumber of the transpiration or boundary wave responsible for the instability can be found where the bifurcation necessarily changes from being subcritical to supercritical. At such points the coefficient of the cubic term in the amplitude equation vanishes and the multiple scale approach must be modified to allow the appearance of quintic terms in the amplitude equation.

Now let us consider the possible practical importance of the problem considered here. Our results show that for a fixed small amplitude wall or transpiration waviness an instability will occur when the Reynolds number is increased to a sufficiently large value. The instability is caused by the interaction of the wave with the underlying shear flow. For Reynolds numbers of the order 10^3 the amplitude of the wall waviness is a tiny frac-

tion of the pipe radius. Or for the transpiration problem the transpiration amplitude is tiny compared to the maximum streamwise velocity. Thus, very small wall undulation or transpiration can generate instability in practically relevant flow regimes.

The wavy wall problem considered can be thought of as a prototype problem to understand the effect of wall roughness on transition to turbulence. But to model the roughness by a single Fourier wave seems at first sight to be a rather optimistic approximation. In fact we can Fourier analyse more complex wall shapes and because the wall waviness within the VWI interaction allows each wave to interact only with itself we can sum over a number of modes and consider more general pipe shapes.

The obvious application of the instability described here is as a means to destabilise laminar flows with a view to enhance mixing. However there is another application in connection with coherent structures. The fundamental building block of exact coherent structures, the roll-streak field, is identical with or without transpiration and is driven by a vortex-wave interaction in both cases. The close relationship of the sustaining mechanisms for exact coherent structures with and without transpiration suggests that transpiration might well have a significant effect on fully turbulent flows. This points to the possible importance of transpiration to control turbulence by preferentially exciting less dissipative underlying flow patterns. Certainly it is now well-established that suction is a viable means to control boundary layer transition but the engineering difficulties associated with producing a wavelike transpiration distribution velocity field are challenging.

Bibliography

Balakumar, P., & Hall, P. (1999). Optimum Suction Distribution for Transition Control. *Theoretical and Computational Fluid Dynamics*, *13*(1), 1–19. https://doi.org/10.1007/s001620050109

Comini, G., Nonino, C., & Savino, S. (2003). Effect of space ratio and corrugation angle on convection enhancement in wavy channels. *International Journal of Numerical Methods for Heat &amp Fluid Flow*, *13*(4), 500–519. https://doi.org/10.1108/09615530310475939

Drazin, P. G. (2002). *Introduction to hydrodynamic stability*. Cambridge University Press. https://doi.org/10.1017/CBO9780511809064

Eckhaus, W. (1965). *Studies in non-linear stability theory*. Springer Berlin / Heidelberg.

Gad-el-Hak, M. (1990). Control of low-speed airfoil aerodynamics. *AIAA Journal*, *28*(9), 1537–1552. https://doi.org/10.2514/3.25250

Glendinning, P. (1994). *Stability, instability and chaos: An introduction to the theory of nonlinear differential equations*. Cambridge University Press. https://doi.org/10.1017/CBO9780511626296

Gülhan, A., & Braun, S. (2010). An experimental study on the efficiency of transpiration cooling in laminar and turbulent hypersonic flows. *Experiments in Fluids*, *50*(3), 509–525. https://doi.org/10.1007/s00348-010-0945-6

Guzmán, M. A., Cárdenas, J. M., Urzúa, A. F., & Araya, E. P. (2009). Heat transfer enhancement by flow bifurcations in asymmetric wavy wall channels. *International Journal of Heat and Mass Transfer*, *52*(15-16), 3778–3789. https://doi.org/10.1016/j.ijheatmasstransfer.2009.02.026

Hall, P. (2020). An instability mechanism for channel flows in the presence of wall roughness. *Journal of Fluid Mechanics*, *899*, R2. https://doi.org/10.1017/jfm.2020.493

Hall, P., & Ozcakir, O. (2021). Poiseuille flow in rough pipes: Linear instability induced by vortex–wave interactions. *Journal of Fluid Mechanics*, *913*, A43. https://doi.org/10.1017/jfm.2021.52

Hall, P., & Smith, F. T. (1991). On strongly nonlinear vortex/wave interactions in boundary-layer transition. *Journal of Fluid Mechanics*, *227*, 641–666. https://doi.org/10.1017/S0022112091000289

Hall, P. (2022). A vortex–wave interaction theory describing the effect of boundary forcing on shear flows. *Journal of Fluid Mechanics*, *932*, A54. https://doi.org/10.1017/jfm.2021.1053

Kandlikar, S. (2008). Exploring roughness effect on laminar internal flow–are we ready for change? *Nanoscale and Microscale Thermophysical Engineering - NANOSCALE MICROSCALE THERMO E*, *12*, 61–82. https://doi.org/10.1080/15567260701866728

Kogelman, S., & DiPrima, R. C. (1970). Stability of spatially periodic supercritical flows in hydrodynamics. *The Physics of fluids (1958)*, *13*(1), 1–11.

Ni, A. (2019). Hyperbolicity, shadowing directions and sensitivity analysis of a turbulent three-dimensional flow. *Journal of Fluid Mechanics*, *863*, 644–669. https://doi.org/10.1017/jfm.2018.986

Ozcakir, O., Hall, P., & Blackburn, H. M. (2022). Exact coherent structures in pipe flow in the presence of wall transpiration. *Journal of Fluid Mechanics*, *940*, A41. https://doi.org/10.1017/jfm.2022.229

Raposo, H., Mughal, S., & Ashworth, R. (2019). An adjoint compressible linearised Navier–Stokes approach to model generation of Tollmien–Schlichting waves by sound. *Journal of Fluid Mechanics*, *877*, 105–129. https://doi.org/10.1017/jfm.2019.601

Ruban, A. I. (1985). On the generation of Tollmien-Schlichting waves by sound. *Fluid Dynamics*, *19*(5), 709–717. https://doi.org/10.1007/bf01093536

Smith, F. T. (1982). On the High Reynolds Number Theory of Laminar Flows. *IMA Journal of Applied Mathematics*, *28*(3), 207–281. https://doi.org/10.1093/imamat/28.3.207

Stuart, J. T. (1971). Nonlinear stability theory. *Annual Review of Fluid Mechanics*, *3*(1), 347–370. https://doi.org/10.1146/annurev.fl.03.010171.002023

Taylor, G. I. (1923). VIII. stability of a viscous liquid contained between two rotating cylinders. *Philosophical Transactions of the Royal Society of London. Series A, Containing Papers of a Mathematical or Physical Character*, *223*(605-615), 289–343. https://doi.org/10.1098/rsta.1923.0008

Appendix

The $O(\delta^3 A^3)$ velocity field from section 2.3 is

$$u_{31}(y) = \frac{1}{98304k^4}e^{-3ky}\Big(- 6039 - 3e^{2ky}(-2013 - 284F_2(-4+ky)+ \\ 4ky(-37 + 2048F3k(1+ky))) + 384F_2(12 + ky(25 + 2ky(15+8ky)))- \\ 8ky(1467 + 2ky(663 + 2ky(175 + 46ky)))\Big), \tag{4.0.1}$$

$$v_{31}(y) = \frac{1}{4096k^2}e^{-3ky}\Big(37 + 32F_2(3+4ky) + 4ky(13+6ky)+ \tag{4.0.2}$$

$$e^{2ky}(-37 - 96F_2 + 4096F_3k^2y)\Big), \tag{4.0.3}$$

$$w_{31}(y) = \frac{1}{4096k^2}e^{-3ky}\Big(59 + 160F_2 + 12ky(9 + 32F_2 + 6ky)+ \\ e^{2ky}(-37 - 96F_2 + 4096F_3k(-1+ky))\Big), \tag{4.0.4}$$

and the velocity field of $O(\delta^3 A')$ from the same section turns out to be

$$u_{33}(y) = \frac{e^{-ky}y\Big(15 - 12F_3k(1+ky) + ky(15+4ky)\Big)}{48k^3}, \tag{4.0.5}$$

$$v_{33}(y) = -\frac{e^{-ky}y(2 - F_3k + ky)}{4k}, \tag{4.0.6}$$

$$w_{33}(y) = \frac{e^{-ky}\Big(2 - k^2y^2 + 4F_3k(-1+ky)\Big)}{4k^2}. \tag{4.0.7}$$

From section 2.4.1 the last Q wave pressure term is

$$Q_3 = -\frac{1}{216(\alpha^2+k^2)}\Big((360\hat{\Gamma}\lambda_1 - 10\lambda_1^3 + 360(\lambda_{31}+\lambda_{33}) - 81k^2\lambda_1^2Q_1+ \tag{4.0.8}$$

$$324k^2\lambda_2Q_1 + 12\lambda_1(10\lambda_2 + 20\lambda_M + 27k^2Q_2)\Big), \tag{4.0.9}$$

and the last Q wave pressure term for the transpiration case from 2.4.2 is

$$Q_3 = -\frac{1}{8(\alpha^2+k^2)}\Big)8\lambda_{31} + 8\lambda_{33} + 8\lambda_1\hat{\Lambda} - 3k^2\lambda_1^2Q_1 + 12k^2\lambda_2Q_1 + 12k^2\lambda_1Q_2. \tag{4.0.10}$$

We now advance to the Chapter 2 terms. From section 3.3 the $O(\delta^2)$ terms are

$$u_2(r) = -\frac{r^{-1+2M}}{8(1+2M)}(-1+r^2)\Big(-8(L_2+2L_2M)+L_1^2(1+r^2)\Big), \tag{4.0.11}$$

$$\begin{aligned} v_2(r) = \frac{1}{8M(1+2M)}\Big(r^{-1+2M}(L_1^2(-M+(2+M)r^4) \\ -8L_2(1+2M)(r^2+M(-1+r^2)))\Big), \end{aligned} \tag{4.0.12}$$

$$\begin{aligned} &w_2(r) = -\frac{1}{96(1+M)(2+M)(1+2M)^2(3+2M)} \\ &\Big(r^{2M}(-1+r^2(L_1^2(43+98+68M^2+16M^3-(1+2M)(11+2M(12+5M))r^2 \\ &+2(-1+M)(1+M)(1+2M)r^4)+ \\ &12L_2(2+M)(1+2M)(3+2M)(-3+r^2+2M(-1+r^2))))\Big), \end{aligned} \tag{4.0.13}$$

$$\begin{aligned} w_M(r) = \frac{1}{16M(3+M)}\Big(-2(9+5M)+r^{2M}(-L_1(3+M)^2- \\ M(2+M)(3+M)(7+3M)r^2+M(1+M)(3+M)(5+3M)r^4+ \\ L_1M(1+M)r^6)\Big). \end{aligned} \tag{4.0.14}$$